The Astrophysical Journal, 948:67 (11pp), 2023 May 1 https://doi.org/10.3847/1538-4357/acc178

A Nonrepeating Fast Radio Burst in a Dwarf Host Galaxy

Shivani Bhandari[1,2,3,17], Alexa C. Gordon[4], Danica R. Scott[5], Lachlan Marnoch[3,6,7,8], Navin Sridhar[9,10], Pravir Kumar[11,12], Clancy W. James[5], Hao Qiu[13], Keith W. Bannister[3], Adam T. Deller[11], Tarraneh Eftekhari[4,18], Wen-fai Fong[4], Marcin Glowacki[5], J. Xavier Prochaska[14,15,16,19], Stuart D. Ryder[6,7], Ryan M. Shannon[11], and Sunil Simha[14]

[1] ASTRON, Netherlands Institute for Radio Astronomy, Oude Hoogeveensedijk 4, 7991 PD Dwingeloo, The Netherlands; bhandari@astron.nl
[2] Joint institute for VLBI ERIC, Oude Hoogeveensedijk 4, 7991 PD Dwingeloo, The Netherlands
[3] CSIRO, Space and Astronomy, P.O. Box 76, Epping, NSW 1710 Australia
[4] Center for Interdisciplinary Exploration and Research in Astrophysics (CIERA) and Department of Physics and Astronomy, Northwestern University, Evanston, IL 60208, USA
[5] International Centre for Radio Astronomy Research (ICRAR), Curtin University, Bentley, WA 6102, Australia
[6] School of Mathematical and Physical Sciences, Macquarie University, Sydney, NSW 2109, Australia
[7] Astronomy, Astrophysics and Astrophotonics Research Centre, Macquarie University, Sydney, NSW 2109, Australia
[8] ARC Centre of Excellence for All-Sky Astrophysics in 3 Dimensions (ASTRO 3D), ACT 2601, Australia
[9] Department of Astronomy, Columbia University, New York, NY 10027, USA
[10] Theoretical High Energy Astrophysics (THEA) Group, Columbia University, New York, NY 10027, USA
[11] Centre for Astrophysics and Supercomputing, Swinburne University of Technology, John St, Hawthorn, VIC 3122, Australia
[12] Department of Particle Physics and Astrophysics, Weizmann Institute of Science, Rehovot 7610001, Israel
[13] SKA Observatory, Jodrell Bank, Lower Withington, Macclesfield, SK11 9FT, UK
[14] University of California—Santa Cruz 1156 High St. Santa Cruz, CA 95064 USA
[15] Kavli IPMU (WPI), UTIAS, The University of Tokyo, Kashiwa, Chiba 277-8583, Japan
[16] Division of Science, National Astronomical Observatory of Japan,2-21-1 Osawa, Mitaka, Tokyo 181-8588, Japan
Received 2022 November 30; revised 2023 March 3; accepted 2023 March 3; published 2023 May 8

Abstract

We present the discovery of an as yet nonrepeating fast radio burst (FRB), FRB 20210117A, with the Australian Square Kilometre Array Pathfinder (ASKAP), as a part of the Commensal Real-time ASKAP Fast Transients Survey. The subarcsecond localization of the burst led to the identification of its host galaxy at $z = 0.214(1)$. This redshift is much lower than what would be expected for a source dispersion measure (DM) of 729 pc cm^{-3}, given typical contributions from the intergalactic medium and the host galaxy. Optical observations reveal the host to be a dwarf galaxy with little ongoing star formation—very different to the dwarf host galaxies of the known repeating FRBs 20121102A and 20190520B. We find an excess DM contribution from the host and attribute it to the FRB's local environment. We do not find any radio emission from the FRB site or host galaxy. The low magnetized environment and the lack of a persistent radio source indicate that the FRB source is older than those found in other dwarf host galaxies, establishing the diversity of FRB sources in dwarf galaxy environments. We find our observations to be fully consistent with the "hypernebula" model, where the FRB is powered by an accretion jet from a hyperaccreting black hole. Finally, our high time resolution analysis reveals burst characteristics similar to those seen in repeating FRBs. We encourage follow-up observations of FRB 20210117A to establish any repeating nature.

Unified Astronomy Thesaurus concepts: Radio transient sources (2008); Dwarf galaxies (416); High time resolution astrophysics (740); High energy astrophysics (739)

1. Introduction

Fast radio bursts (FRBs) are pulses of coherent radio emission with nano- to millisecond durations and dispersion measures (DMs) exceeding the maximum expected contribution from the Milky Way along a given line of sight (Petroff et al. 2016). The majority of the published sample of >600 FRBs are dominated by nonrepeating events; only 4% of FRB sources are observed to emit repeating bursts (Amiri et al. 2021). While the fundamental relationship between repeating and nonrepeating FRBs is unknown, the growing sample reveals statistical differences in the burst properties of the two speculative populations (Pleunis et al. 2021). There are, however, no significant differences between the galaxies hosting repeating and nonrepeating FRBs (Bhandari et al. 2022). The localized sample of 22 FRBs mostly come from the outskirts of their host galaxies, at redshifts ranging from less than 0.001 to 1.016, and they have diverse host and local environments (Tendulkar et al. 2017; Ravi et al. 2019; Bhandari et al. 2020; Heintz et al. 2020; Marcote et al. 2020; Fong et al. 2021; Bhandari et al. 2022; Kirsten et al. 2022; Niu et al. 2022; Ravi et al. 2022; Ryder et al. 2022).

The first repeating FRB 20121102A (Spitler et al. 2016) is localized to a low-metallicity dwarf host galaxy with a high specific star formation rate (SFR), at $z = 0.192$ (Tendulkar et al. 2017). The burst was found to be colocated with a compact persistent radio source (PRS; <0.7 pc in size), suggesting that the FRB source is embedded in a radio nebula (Chatterjee et al. 2017; Marcote et al. 2017). Also, the repeat

[17] Veni Fellow.
[18] NHFP Einstein Fellow.
[19] Simons Pivot Fellow.

bursts were observed to have an exceptionally high ($\sim 10^5$ rad m^{-2}) and highly variable rotation measure (RM; Michilli et al. 2018; Hilmarsson et al. 2021). The properties of the local environment and host galaxy of FRB 20121102A led to a concordant model for FRBs, in which bursts are produced by young magnetars, which are themselves produced in superluminous supernovae (SLSNe) or long gamma-ray bursts (LGRBs; Margalit & Metzger 2018). Alternatively, the PRS can also be self-consistently explained by an accreting compact object engine (Chen et al. 2022; Sridhar & Metzger 2022).

More recently, the repeating FRB 20190520B was discovered using the FAST radio telescope. The observed DM of 1202 pc cm^{-3} would imply a redshift of $z \gtrsim 1$ (Macquart et al. 2020). Surprisingly, however, the localization of the FRB and optical observations revealed a dwarf host galaxy at $z = 0.241$, making this source the FRB with the highest host DM contribution, of $\mathrm{DM_{host}} = 903^{+72}_{-111}$ pc cm^{-3} (Niu et al. 2022). This is unlikely to be due to the interstellar medium (ISM) of the host galaxy, but rather more plausibly to be due to the local environment of the source. This host DM is a factor of $\sim$5 larger than what has been observed for FRB host galaxies (James et al. 2022a), and a factor of a few beyond what has been estimated for FRB 20121102A (Tendulkar et al. 2017). Interestingly, similar to FRB 20121102A, FRB 20190520B is colocated with a PRS (only the second ever to be found). Furthermore, that these two FRBs are among the active repeating sources and also linked with PRSs implies that they may be characteristic of young and active FRB sources that are surrounded by dense and magnetized plasma.

Alternatively, other FRBs have been found in massive and moderately star-forming galaxies lacking a strong magnetic environment and radio nebula. It is possible that such sources are relatively older or live in less dense environments, leading to an underluminous PRS (Margalit et al. 2019; Sridhar & Metzger 2022). Also, a CHIME/FRB repeating source, FRB 20200120E, was recently localized to a globular cluster in the galaxy M81, revealing a very different local environment for this source (Kirsten et al. 2022).

It is appealing to explain the wide variety of FRB environments by means of a connected mechanism, which is typically attributed to either the source age or the source formation channel. In either case, knowledge of the environments surrounding a larger sample of FRBs is key to understanding this potential connection. The presence or absence of a PRS or radio emission from star formation, and how it correlates with FRB properties—such as the repetition rate, the DM due to the host galaxy, the RM, etc.—is therefore critical.

In this paper, we present the discovery of the apparently nonrepeating FRB 20210117A, with the Australian Square Kilometre Array Pathfinder (ASKAP), and its localization to a dwarf galaxy. Section 2 describes the discovery as well as the properties of the host galaxy. Section 3 presents the high time resolution analysis of the burst. Section 4 describes the follow-up radio observations that were made to look for a PRS and repeating bursts from the source of FRB 20210117A. Section 5 discusses the implications of our findings, and Section 6 provides a summary.

2. Discovery of FRB 20210117A

The burst was detected on 2021 January 17, UT 07:51:21.277, in the real-time CRAFT incoherent sum search observations, using 26 ASKAP dishes, at a center frequency of 1271.5 MHz, spanning a bandwidth of 336 MHz. These observations were simultaneously carried out with the Rapid ASKAP Continuum Survey (RACS; McConnell et al. 2020) observations. The burst, however, was not detected in a 10 s commensal ASKAP snapshot, taken during an RACS pointing of 15 minutes. In the CRAFT data, the burst had a maximum signal-to-noise ratio (S/N) of 27.1 in the outer ASKAP beam, 02, and it was also detected in beams 01 and 07, with S/Ns of 16.3 and 4.7, respectively, with the closepack36 beam footprint pattern (see Shannon et al. 2018). The burst has a fluence of 36^{+28}_{-9} Jy ms^{-1} and a structure-maximized DM of $729.1^{+0.36}_{-0.23}$ pc cm^{-3}, which was derived using the method described in Sutinjo et al. (2023). The k-corrected isotropic equivalent spectral energy of the burst is derived using

$$E_\nu = \frac{4\pi\, D_L(z)^2}{(1+z)^{2+\alpha}}\, F_\nu, \tag{1}$$

where $D_L(z)$ is the luminosity distance, F_ν is the burst fluence, and α is the spectral index ($F \propto \nu^\alpha$; James et al. 2022b). We use a default value of $\alpha = -1.5$ (Macquart et al. 2019), and derive $E_\nu = 4.6 \times 10^{31}$ erg Hz^{-1}. We note that any beaming of the FRB can reduce this energy budget by a factor of $\Delta\Omega/4\pi$, where $\Delta\Omega$ is the unknown beaming solid angle. Furthermore, if beaming is invoked to reduce the energy of a burst, this implies that such bursts are more numerous, as we only see a fraction of them. The other measured and derived properties of FRB 20210117A are listed in Table 1.

The detection in the real-time system triggered a download of 3.1 s of voltages around the time of the FRB. Using the standard CRAFT post-processing pipeline (Day et al. 2020), we imaged both the FRB and the continuum sources visible in the field. The FRB was detected with a significance of 50 σ, leading to a statistical positional precision of $\sim 0\farcs1$ in R.A. and decl. We used the method described in Day et al. (2021) to estimate the systematic uncertainties, by identifying seven compact sources greater than 7σ in the 3 s field image and comparing them to their counterparts in the RACS radio image. We obtained an offset correction of $0\farcm02 \pm 0\farcm08$ in R.A. and $0\farcs01 \pm 0\farcs08$ in decl. The final burst position is R.A.(J2000): $22^{\mathrm{h}}39^{\mathrm{m}}55\fs015$ and decl.(J2000): $-16°09\farcm05\farcs45$, with an uncertainty of $0\farcs13 \times 0\farcs12$.

2.1. Host Galaxy of FRB 20210117A

On 2021 June 10/11, we used Keck/DEIMOS to image the field in the r band. The data revealed a faint galaxy with $r \sim 23$, coincident with the position of the burst. We performed a probabilistic association of transient hosts (Aggarwal et al. 2021) analysis, which yielded a posterior probability of $P(O|x) = 0.9984$ of this source being the host of FRB 20210117A.

On 2021 June 12 UT, additional imaging observations in the g and I bands were obtained using the FORS2 instrument mounted on Unit Telescope 1 (UT1) of the European Southern Observatory's Very Large Telescope (ESO VLT). The images were processed as described by Marnoch et al. (2020): debiasing and flatfielding were carried out using ESOReflex[20] (Freudling et al. 2013); mosaicing was done with Montage[21] (Berriman & Good 2017); and astrometric calibration was done

[20] https://www.eso.org/sci/software/esoreflex/
[21] http://montage.ipac.caltech.edu/

Table 1
Measured and Derived Properties of FRB 20210117A and Its Host Galaxy

Measured Burst Properties	
Arrival Time at 1271.5 MHz	2021-01-17-07:51:21.277
S/N	27.0
Structure-maximized DM (pc cm^{-3})	$729.1^{+0.36}_{-0.23}$
DM_{ISM} NE2001 (pc cm^{-3})	34
DM_{ISM} YMW16 (pc cm^{-3})	23
DM_{cosmic}(pc cm^{-3})	$\sim$184
DM_{host}(pc cm^{-3})	$\sim$460
R.A. (J2000)	22h39m55.015(9)s
Decl. (J2000)	$-16°09'05''.45(12)$
Fluence (Jy ms^{-1})	36^{+28}_{-9}
Peak1 pulse width (ms)[a]	0.14 ± 0.01
Peak2 pulse width (ms)[a]	0.17 ± 0.02
Precursor component pulse width (ms)[a]	0.53 ± 0.03
Scattering time ($\tau_{1.2\ GHz}$) (ms)	0.33 ± 0.02
RM (rad m^{-2})	43 ± 0.6
Spectral energy density (erg Hz^{-1})	4.6×10^{31}
PRS luminosity ($L_{6\ GHz}$) (W Hz^{-1})	$<1.5 \times 10^{21}$
Host galaxy properties	
R.A. (J2000)	22h39m55.07(2)s
Decl. (J2000)	$-16°09'05''37(2)$
Redshift	0.214(1)
g (AB mag)	23.60 ± 0.02
r (AB mag)	22.97 ± 0.04
I (AB mag)	22.23 ± 0.05
J (AB mag)	22.69 ± 0.08
H (AB mag)	22.94 ± 0.1
K (AB mag)	22.80 ± 0.1
u–r (rest-frame)	1.0 ± 0.1
M_r (rest-frame)	-17.23 ± 0.05
$\log(M_*/M_\odot)$	$8.56^{+0.06}_{-0.08}$
100 Myr SFR ($M_\odot$ yr^{-1})	$0.014^{+0.008}_{-0.004}$
log(sSFR) (yr^{-1})	-10.4
Mass-weighted age (Gyr)	$5.06^{+0.91}_{-1.34}$
Projected offset from galaxy center (kpc)	2.8 ± 0.4

Notes.
[a] The reported widths are 1σ of the Gaussian.

using a local installation of Astrometry.net[22] (Lang et al. 2010), incorporating the Gaia (Lindegren et al. 2018) catalog—this resulted in a precision (calculated as the rms of the offsets of the imaged stars from counterparts in Gaia Data Release 3) of $\sim$0.″07 for both bands. The g-band image was calibrated photometrically against Data Release 2 of the DELVE catalog (Drlica-Wagner et al. 2022), and the I-band image was calibrated using the FORS2 Quality Control archive. The total integration times and image qualities were 5000/900 s and 0.″70/0.″65 for g/I, respectively. Further imaging was acquired on 2022 June 10 UT, with the HAWK-I instrument, on UT4 of the ESO VLT, in the J, H, and Ks bands. ESOReflex was used for the debiasing, flatfielding, and coaddition of the images, while photometric calibration was performed against the Two Micron All Sky Survey Point-Source Catalog (Skrutskie et al. 2006). The astrometric calibration was performed using the same procedure, with FORS2. Each band was observed for a total integration time of 750 s. See Table 1 for the photometric details.

[22] http://astrometry.net/

2.1.1. Host Galaxy Spectrum

Having identified the most likely host galaxy in these images (Figure 1), follow-up spectroscopy using FORS2—with a 1″ slit, the GRIS300I grism, and the OG590 order sorting filter—was obtained on 2021 September 6 UT. This yielded wavelength coverage of 600–1100 nm at a resolution of 660. The total on-source exposure time was 2600 s.

The spectrum was reduced with the Python Spectroscopic Data Reduction Pipeline (`PypeIt`; Prochaska et al. 2020). `PypeIt` performed flatfielding, bias subtraction, wavelength calibration, and spectral extraction, using the standard default parameters. The spectrum was then flux-calibrated using the spectrophotometric standard star EG21, which was observed on 2021 September 2 UT. The two 1300 s exposures were combined via 1D coaddition and scaled to match the Keck/DEIMOS r-band flux. Finally, the spectrum was telluric-corrected, using the Paranal VIS 4900 atmospheric grid, and corrected for extinction, using the Calzetti (2001) extinction law. Detections of the Hα, [S II] doublet and [O III] doublet spectral lines confirmed the redshift of the host to be $z = 0.214$ (1). No other spectral lines are apparent in the data.

2.1.2. Stellar Population Modeling

To determine the stellar population properties of the host galaxy, the stellar population synthesis modeling code `Prospector` (Johnson et al. 2021) was used. The observed photometry and spectroscopy were jointly fit using the stellar population synthesis library `python-fsps` (Conroy et al. 2009; Conroy & Gunn 2010). We assume a Kroupa (2001) initial mass function and a Kriek & Conroy (2013) dust attenuation curve. The additional assumed priors included a ratio on the dust attenuation between old and young stars, a mass–metallicity relationship (Gallazzi et al. 2005), and a continuity nonparametric star formation history (Leja et al. 2019), using eight age bins. Several spectroscopic calibration parameters were used, including a spectral smoothing parameter, a parameter to normalize the spectrum to the photometry, a pixel outlier model to marginalize over poorly modeled noise, and a jitter model to inflate the noise in all spectroscopic pixels, to ensure a better fit between the model and observed spectrum. A twelfth-order Chebyshev polynomial was then used to fit the spectral continuum. Our assumed model, as described above, was then sampled using the dynamic nested sampling routine `dynesty` (Speagle 2020), to produce the posterior distributions of the stellar population parameters.

The resulting model reveals a dwarf galaxy with a stellar mass of $\log(M_*/M_\odot) = 8.56^{+0.06}_{-0.08}$ and a mass-weighted age of $5.06^{+0.91}_{-1.34}$ Gyr (Gordon et al. 2023), a metric that is less biased by the youngest and brightest stars in the galaxy, compared to traditional light-weighted ages (Conroy 2013). The host has a low current SFR, with an average SFR over the past 100 Myr of $0.014^{+0.008}_{-0.004}$ $M_\odot$ yr^{-1}. These values and the other host properties are reported in Table 1. We note that as `prospector` is a Bayesian inference code, the uncertainties on the stellar parameters correspond to the 68% confidence intervals on the posteriors, given all the priors for the assumed model.

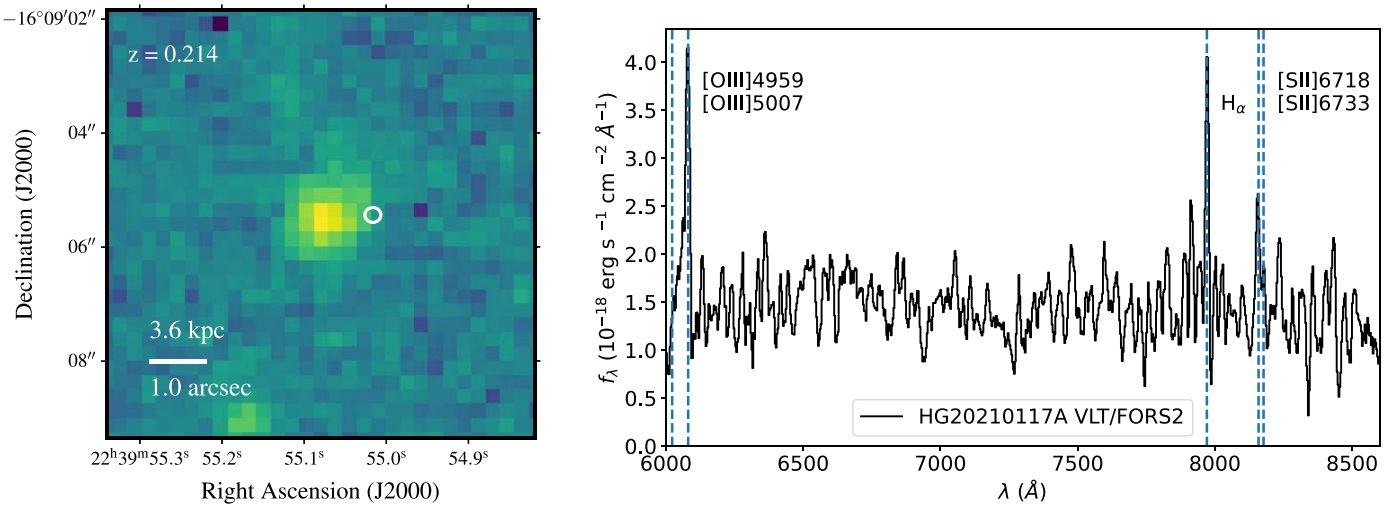

Figure 1. Left: *I*-band VLT/FORS2 image of the host galaxy of FRB 20210117A, overplotted with the position of the burst. The white circle represents the total uncertainty (1σ) in the FRB position. Right: VLT/FORS2 spectrum of the FRB 20210117A host galaxy, which is used to estimate the redshift of the host as $z = 0.214$.

2.2. Excess Host DM

The observed DM of the FRB can be divided into contributions from various components, as

$$\mathrm{DM_{obs}} = \mathrm{DM_{MW,ISM}} + \mathrm{DM_{MW,halo}} + \mathrm{DM_{EG}}$$
$$\mathrm{DM_{EG}} = \mathrm{DM_{cosmic}} + \frac{\mathrm{DM_{host}}}{1+z}. \quad (2)$$

Here, $\mathrm{DM_{MW,ISM}}$ and $\mathrm{DM_{MW,halo}}$ are the contributions due to the Milky Way's ISM and halo. These are estimated to be 34 pc cm^{-3} and 23 pc cm^{-3} from the Galactic models of NE2001 (Cordes & Lazio 2002) and YMW16 (Yao et al. 2017), respectively, and $\mathrm{DM_{MW,halo}}$ is assumed to be 50 pc cm^{-3} (Prochaska & Zheng 2019). $\mathrm{DM_{EG}}$ refers to the extragalactic DM that is composed of the contributions due to the intergalactic medium (IGM)/foreground halos along the FRB sightline ($\mathrm{DM_{cosmic}}$) and the host galaxy of the FRB ($\mathrm{DM_{host}}$). $\mathrm{DM_{cosmic}}$ is estimated to be 183 pc cm^{-3} using the Macquart (DM–z) relation (Macquart et al. 2020). After subtracting the respective contributions of the Milky Way (using NE2001) and IGM from the observed DM of the FRB, we find $\mathrm{DM_{host}}$ to be $\sim$460 pc cm^{-3}, which is greater than what has been observed for ASKAP-localized FRBs (a median of $\mathrm{DM_{host}} = 186^{+59}_{-48}$ pc cm^{-3}; James et al. 2022a). A much lower value is possible if the sightline exhibits a higher $\mathrm{DM_{cosmic}}$ value than is typical; see Simha et al. (2023) for such a test hypothesis. When we include the variation in $\mathrm{DM_{cosmic}}$ from Macquart et al. (2020), with a feedback parameter $F = 0.32$, in Equation (2), we produce a distribution for $\mathrm{DM_{host}}$. Scaling this to the host galaxy rest frame by $1+z$, as per Ryder et al. (2022), produces Figure 2, where the rest-frame DM is compared to those of other FRBs with large $\mathrm{DM_{host}}$ contributions. Using this method, we estimate the median rest-frame $\mathrm{DM_{host}}$ for FRB 20210117 to be 595^{+55}_{-24} pc cm^{-3}.

James et al. (2022b) demonstrated that it is critical to consider observational biases in a survey, because they can result in an inversion of the Macquart relationship, after a certain DM value. Using their $P(\mathrm{DM_{EG}},z)$ grid for the CRAFT/incoherent sum (ICS) survey, we calculate the probability distribution function (PDF), $P(\mathrm{DM_{EG}}|z)$, given the redshift of FRB 20210117A. The PDF is presented in Figure 3, reaching its maximum at an extragalactic DM of 182 pc cm^{-3}, with a 1σ confidence interval spanning 176–496 pc cm^{-3}. We also show the PDF of the DM due to the IGM and the extragalactic DM, both of which are free of any instrumental biases.

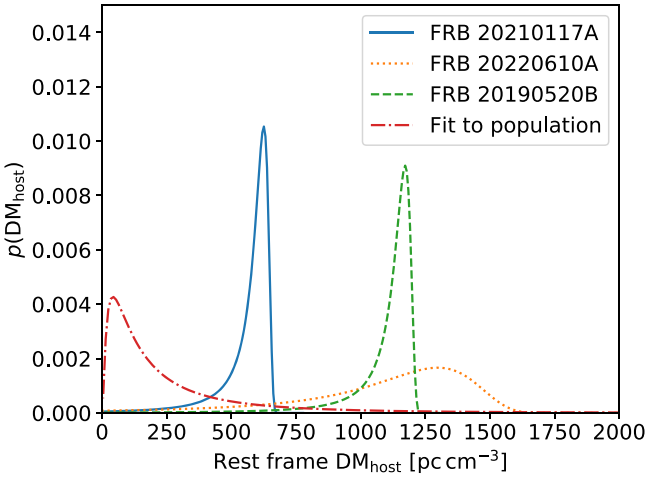

Figure 2. Probability density functions $\mathrm{P(DM_{host})}$ for the host galaxy DM contribution, scaled by $1+z$ to the host galaxy's rest frame. Values are shown for three localized FRBs—blue solid line: FRB 20210117; green dashed line: FRB 20190520B (Niu et al. 2022); and orange dotted line: FRB 20220610A (Ryder et al. 2022)—as well as the log-normal fit to the FRB population, based on ASKAP and Parkes (Murriyang) data (James et al. 2022b).

The host DM contribution can be probed by optical studies. We use the Hα flux measurement from the spectrum of the host to constrain the host DM. We measure $F_{\mathrm{H}\alpha} = 1.7 \times 10^{-17}$ erg cm^{-2} s^{-1} and use it to derive the Hα luminosity of $L_{\mathrm{H}\alpha} = 2.3 \times 10^{39}$ erg s^{-1}. Dwarfs of the Magellanic type range in size from 1 to 5 kpc (Kaisin et al. 2012). For simplicity, we assume the size of the dwarf host galaxy to be 3 kpc, as we are unable to fit a Sérsic profile, due to galaxy's unresolved nature. Third, the Hα luminosity is proportional to $\int n_e^2\, dV$, because it is a tracer of ionized hydrogen, implying that the free electron density is proportional to the square root of the total Hα

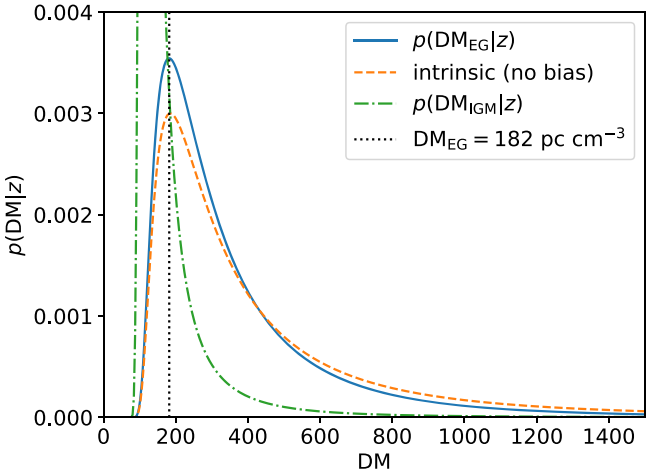

Figure 3. PDF, $P(\mathrm{DM_{EG}}|z)$, for the extragalactic contribution to the DM, given the redshift of the FRB host galaxy. The ASKAP ICS survey yields the blue curve, after accounting for the various survey biases (the peak is shown by the vertical dashed line). The green curve represents the PDF of the DM due to the IGM only (i.e., without the host galaxy), while the orange curve represents the extragalactic DM free of instrumental biases.

luminosity emitted by the host galaxy, $n_e \propto \sqrt{L_{H\alpha}/V}$ (Xu & Han 2015), where V is the volume of a sphere. We note that this assumes that the volumes of galaxies like the Milky Way and dwarfs are uniformly ionized. According to the statistics for Milky Way–type galaxies (James et al. 2004), the total $L_{H\alpha}$ from the Milky Way is $\sim 10^{40}$ erg s^{-1} and the size of the Milky Way is 30 kpc. Finally, using the above relation, we obtain

$$\frac{n_{e,host}}{n_{e,MW}} \propto \sqrt{\frac{L_{H\alpha,host}/V_{host}}{L_{H\alpha,MW}/V_{MW}}},$$
$$\frac{DM_{host}}{DM_{MW}} = \frac{n_{e,host}}{n_{e,MW}} \cdot \frac{l_{host}}{l_{MW}},$$
$$DM_{host} \propto DM_{MW}\left(\frac{L_{H\alpha,host}}{L_{H\alpha,MW}}\right)^{1/2}\left(\frac{R_{MW}}{R_{host}}\right)^{3/2}\left(\frac{l_{host}}{l_{MW}}\right). \quad (3)$$

Here, l_{host} and l_{MW} are the path lengths along the host and the Milky Way, which are assumed to be twice the effective radius of the galaxy. Using the DM_{MW} contribution from NE2001, we estimate DM_{host} to be ~ 60 pc cm^{-3}. We are unable to estimate the host's inclination angle, because the galaxy is barely resolved in our observations. Nevertheless, we note that in a simulation to model the DM due to dwarf galaxies, Xu & Han (2015) found the DM to be 11–12 pc cm^{-3}, 22–24 pc cm^{-3}, and about 100 pc cm^{-3} for inclination angles of 0°, 60°, and 90° respectively. Thus, we conclude that the host ISM alone cannot dominate the excess DM observed along the FRB sightline, and that the excess DM must come from the local environment of FRB 20210117A.

3. High Time Resolution Studies

Using the CRAFT voltage data, we performed a high time resolution analysis of the FRB. The data were beam-formed (coherently summed) at the position of the burst, using the delay, bandpass, and phase solutions derived from the calibrator source PKS 0407−658. The 336 ASKAP channels of 1 MHz bandwidth containing the FRB signal were then coherently dedispersed at the FRB's structure-maximized DM, and passed through a synthesis filter to reconstruct a single 336 MHz channel with ∼3 ns time resolution. Cho et al. (2020) provide a detailed description of the high time resolution construction process.

Next, we characterize the spectral modulation in the burst, which could be intrinsic to the burst emission or caused by propagation effects. The autocorrelation function (ACF) of the main component of the burst spectra $S(\Delta\nu)$ with a frequency resolution of 1 MHz is calculated as follows:

$$A(\delta\nu) = \frac{1}{N}\sum_{\nu} \Delta S(\nu)\Delta S(\nu+\delta\nu), \quad (4)$$

where $\Delta S(\nu) = S(\nu) - \bar{S}$, $\bar{S}$ is the mean spectral power and N is the number of frequency bins (Salpeter 1966). The ACF was then normalized by its maximum and fitted with a one-component Gaussian function from the `lmfit` python package. The central peak FWHM is 103 ± 4 MHz, which is the characteristic frequency scale seen on the spectrum of the burst's main component. The fitted Gaussian function is then subtracted from the ACF, and the residuals are fitted with a Lorentzian function of the following form:

$$f(\delta\nu) = C\left(1 + \frac{\delta\nu^2}{\delta\nu_d^2}\right)^{-1}, \quad (5)$$

where C is a constant and $\delta\nu_d$ is the scintillation bandwidth (see Figure 4). We estimate $\delta\nu_d \sim 6$ MHz, which is consistent with the expectations for diffractive scintillation from the Milky Way along the burst's line of sight, using the NE2001 model (∼3 MHz at 1 GHz).

We fit the frequency-averaged pulse profile with scatter-broadened Gaussian pulse models, using the nested sampling presented in Qiu et al. (2020) and Cho et al. (2020). This allows the fitting of multiple pulse components within the spectrum, as demonstrated in Day et al. (2020).

We model the burst using a three-component scattered pulse with a precursor component (see Figure 5). The fitting of the averaged pulse profile gives a scattering time of $\tau = 0.33 \pm 0.02$ ms at the center frequency of 1271 MHz, assuming $\tau \propto \nu^{-4}$. We note that the scattering fit was performed on the dynamic spectrum dedispersed at the structure-maximized DM. We also estimate the scattering time as a function of different DM trials between 728.6 and 729.4 pc cm^{-3}, finding a gradient of -76 μs per pc cm^{-3}. We note that the scattering timescale is not consistent with the Milky Way estimate (0.06 μs at 1 GHz) from the NE2001 model. Peak 1 and peak 2 have widths of 0.14 ± 0.01 ms and 0.17 ± 0.02 ms, respectively. The two peaks of the main pulse are separated by 0.60 ms. The precursor emission peak occurs ∼1.5 ms before the main peak, with a pulse width of 0.53 ± 0.03 ms.

3.1. Polarimetry

The FRB data were polarization-calibrated using an observation of the Vela pulsar (PSR J0835−4510), which was observed 3.4 hr after the detection of the FRB. This ASKAP observation was compared to a Parkes radio telescope observation of the Vela pulsar with an accurate polarization calibration in order to determine ASKAP's instrumental leakage parameters (differential gain and phase between the

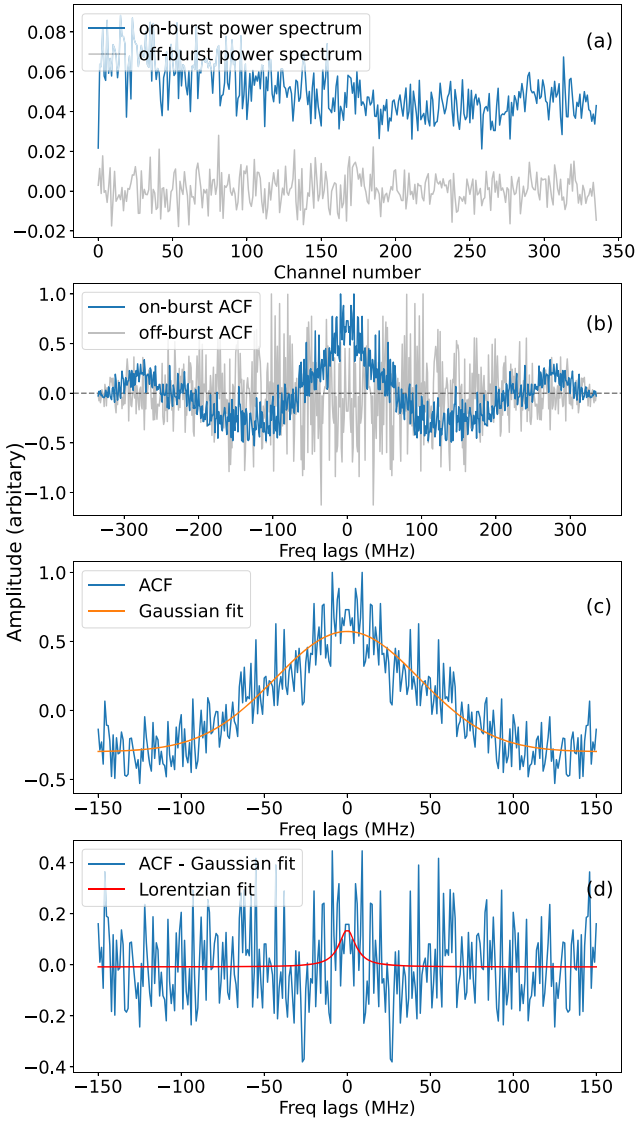

Figure 4. ACF analysis of the time-averaged spectrum of the FRB (resolution = 1 MHz). (a) The burst's on- and off-peak power spectra. (b) The on- and off-peak ACFs. The noise spike with zero lag has been removed. (c) A zoom-in on the peak of the ACF fitted with a one-component Gaussian function. (d) The Lorentzian fit to the residual.

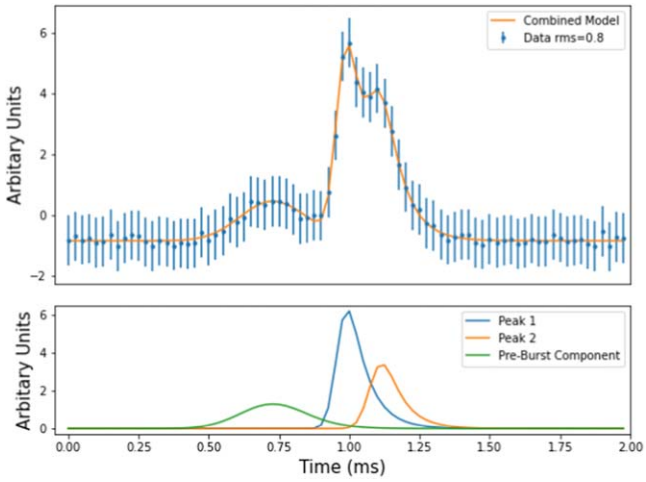

Figure 5. Pulse morphology model plot over a 125 μs time series. The best-fit model comprises a scattered three-component pulse profile.

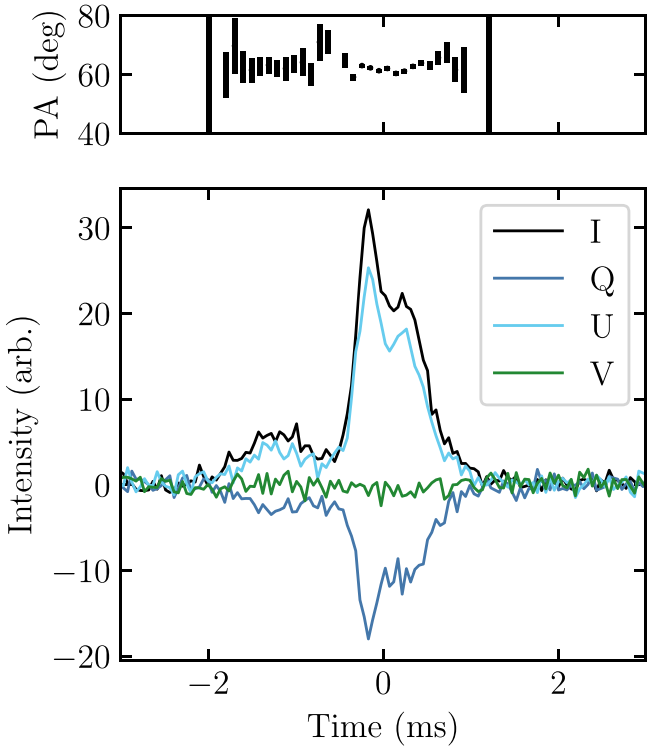

Figure 6. Faraday-corrected profiles of FRB20210117A. Top: polarization PA at a time resolution of 96 μs. Bottom: Stokes profiles at a time resolution of 48 μs.

two linearly polarized receptors), which were then applied to the burst data set. See Day et al. (2021) for additional details.

We used the `RMFIT` program in `PSRCHIVE` to calculate the RM of FRB 20210117A, finding the burst RM to be 43 ± 0.6 rad m^{-2}. The frequency-integrated burst profiles (corrected for Faraday rotation) and the dynamic spectra are presented for all four Stokes parameters, in Figures 6 and 7, respectively. We see a hint of downward drifting structure in the dynamic spectrum, which has now been established as a distinguishing feature of repeating FRBs (Pleunis et al. 2021). Next, we use the method described in Section 2.4.1 of Day et al. (2020) to calculate the polarization position angle (PA) Ψ and the associated uncertainty σ_Ψ, which was estimated using the Faraday-corrected Stokes profiles I, Q, and U. The uncertainties σ_I, σ_Q, and σ_U were estimated by taking the standard deviations of the off-burst Stokes I, Q, and U data. The PA and associated error are shown in the top panel of Figure 6.

We also calculate polarization fractions for the FRB 20210117A time window of 3.6 ms, using the calibrated Stokes parameters. The total debiased linear polarization and the total polarization are given by:

$$L_{\rm de-bias} = \begin{cases} \sigma_I \sqrt{\left(\frac{L_{\rm meas}}{\sigma_I}\right)^2 - 1} & \text{if } \frac{L_{\rm meas}}{\sigma_I} > 1.57 \\ 0 & \text{otherwise.} \end{cases} \quad (6)$$

$$P = \sqrt{L_{\rm de-bias}^2 + V^2}. \quad (7)$$

Here, $L_{\rm meas} = \sqrt{Q^2 + U^2}$. We obtain $L_{\rm de-bias}/I = 0.90$, $V/I = -0.03$, and $P/I = 0.90$.

4. Follow-up Radio Observations

4.1. Search for a PRS

We observed the FRB field with the Karl G. Jansky Very Large Array (VLA), under the project code VLA/20B-103, on 2021 February 20. The source was observed for 52 minutes in the 4–8 GHz frequency band centered at 6 GHz. We also conducted a second epoch of follow-up observations with the Australia Compact Array Telescope, on 2021 September 10, for ∼3 hr, centered at 5.5 GHz and 7.5 GHz. We found no radio emission from anywhere in the host galaxy and no compact PRS at the position of the burst. Our 3σ luminosity limits were 1.5×10^{21} W Hz^{-1} at 6 GHz and 4.0×10^{21} W Hz^{-1} at 6.5 GHz for both epochs, respectively. These limits are lower than the luminosity of the FRB 20121102A PRS (see Table 2), indicating that FRB 20210117A may be an older source or in a less dense environment.

4.2. Search for Repeating Bursts

We conducted follow-up observations of FRB 20210117A using the ultra-wideband low (UWL) receiver at the 64 m Parkes radio telescope (also known as Murriyang). The observations were centered at 2368 MHz, with the bandwidth spanning 0.7 to 4 GHz. The FRB source was observed for a total of 9.2 hr during January and October 2021. We searched the Parkes data for repeat bursts and single pulses, using the `Heimdall` (Barsdell 2012) and `Fetch` (Agarwal et al. 2020) software packages, for a DM range of 100–1100 pc cm^{-3}, utilizing a tiered subband strategy, as described in Kumar et al. (2021). No significant single-pulse candidates of astrophysical origin were identified in these observations above an S/N of 8. We could constrain the detectable fluence of the repeat bursts to $\lesssim$0.15 Jy ms^{-1} in these UWL observations, assuming a broadband pulse (3.3 GHz bandwidth) with a nominal width of 1 ms. If the repeat bursts were narrowband (64 MHz bandwidth), then our search pipeline was sensitive up to ∼1 Jy ms^{-1}. Furthermore, the source was followed up by ASKAP from September 2021 to January 2022, for a duration of 125.53 hr, with the band center frequency ranging from 920.5 to 1632.5 MHz. No significant candidates for repeat bursts were found in these ASKAP observations exceeding a threshold S/N of 10. The ASKAP detection system in the incoherent sum mode is sensitive to a fluence of 3.7 Jy ms^{-1}, for a nominal pulse width of 1 ms, using the entire array of 36 antennas. For most of the follow-up observations, though, smaller subarrays were used, consisting of 23–26 antennas. Assuming a Poissonian rate distribution, we set a 95% upper limit on the burst repetition rate, of $\sim 2.4 \times 10^{-2}$ hr^{-1}, for the ASKAP observations. We note here that in some repeating FRB sources, the burst rate has been found to show significant variations with time as well as frequency (Cruces et al. 2021; Dai et al. 2022; Xu et al. 2022), so this upper limit is just a rough estimate for repetition.

5. Discussion

5.1. Comparison with FRB Host Population

FRB 20210117A is the only published burst to be discovered in a dwarf galaxy where its repeating nature has yet to be established. We compare this source with the published sample of FRB hosts, particularly FRB 20121102A and FRB 20190520B, which are known to originate in dwarf galaxies. Despite the large excess host DM, the local environment of FRB 20210117A differs from those of FRB 20121102A and FRB 20190520B, due to the lack of a

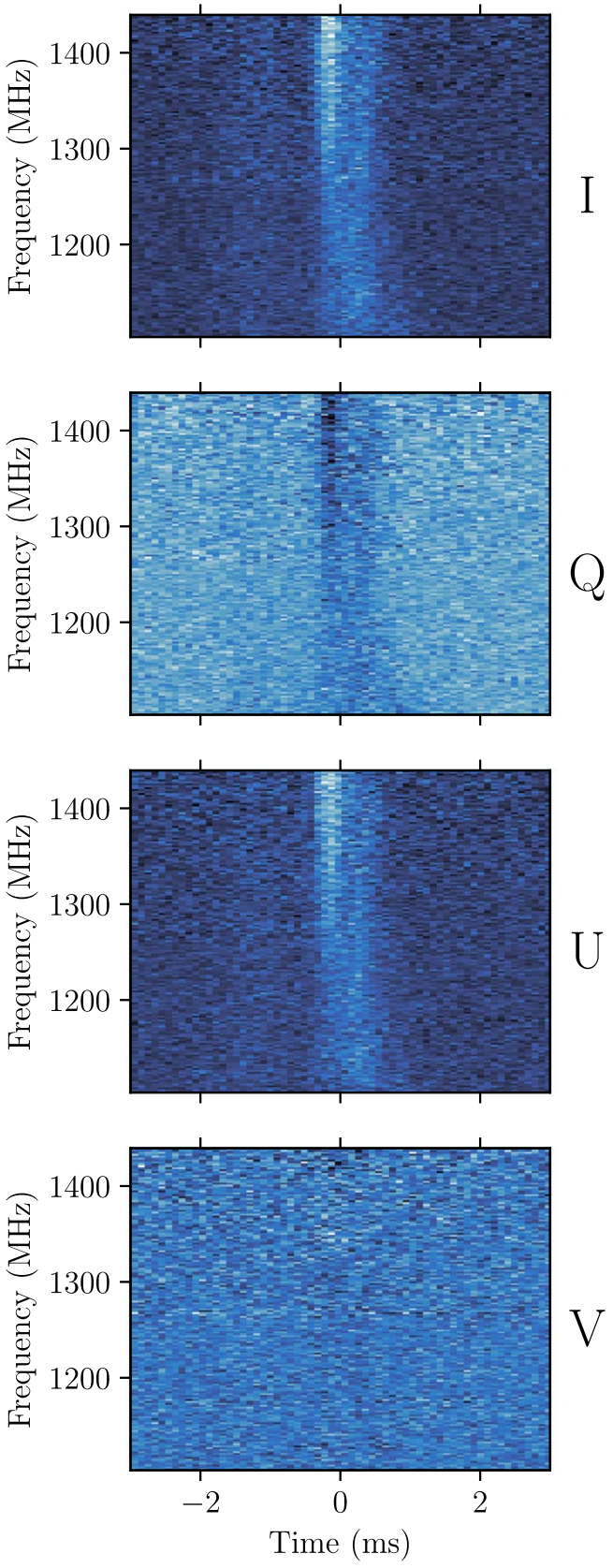

Figure 7. Faraday-corrected Stokes dynamic spectra of FRB20210117A at a time resolution of 96 μs and a frequency resolution of 2 MHz.

Table 2
Observed Properties of FRB 20210117A, along with Those of Two Active Repeating FRBs Localized to Dwarf Galaxies

FRB	z	Repeat Rate (hr^{-1})	RM (rad m^{-2})	PRS Luminosity (W Hz^{-1})	Host DM (pc cm^{-3})	Scattering ($\tau_{1\ GHz}$) (ms)	Pulse Morphology
20121102A	0.192	122	10^5	1.4×10^{22}	$\leqslant 324$	0.02	Repeater-like
20190520B	0.241	$4.5^{1.9}_{-1.5}$	$10^3 - 10^4$	2×10^{22}	903^{+72}_{-111}	24.4	Repeater-like
20210117A	0.214	$<2.4 \times 10^{-2}$	43	$<5.3 \times 10^{21}$	~460	0.86	Repeater-like

Note. The burst rate for 20121102A is the peak rate at 1.25 GHz above a fluence of 0.0015 Jy ms^{-1}, and $R_{=1.2\ GHz}$ (>9.3 mJy ms^{-1}) for 20190520B. We quote the radio luminosities for the PRS at 5 GHz. The properties of FRB 20121102A are taken from Chatterjee et al. (2017), Marcote et al. (2017), Tendulkar et al. (2017), Michilli et al. (2018), Hessels et al. (2019), and Li et al. (2021), while those for FRB 20190520B are taken from Anna-Thomas et al. (2022), Dai et al. (2022), and Niu et al. (2022).

PRS and a low RM, which is suggestive of low magnetic fields or an older system (see Table 2).

We note that FRB 20210117A has the second highest excess DM in the sample of ASKAP-localized bursts, after FRB 20220610A. Simha et al. (2023) have also studied the matter density distribution along the FRB sightline, discovering no foreground galaxies or halos to explain the excess DM. Their study leveraged the spectroscopic redshifts of field galaxies from the FLIMFLAM survey (see Lee et al. 2022) to model the foreground gas distribution from intervening galactic halos, and they also searched for possible galaxy groups whose intergroup medium might contribute to the DM. The resulting empirical model of foreground plasma indicates a very small contribution (<10 pc cm^{-3}) to the DM, and thus also indicates a high host galaxy or progenitor environment value.

We also search for any possible relationships between the scattering and the excess DM for a sample of FRBs, including FRB 20220610A ($\tau_{1\ GHz} = 0.89$ ms; Ryder et al. 2022) and those presented in Table 2. Except for FRB 20121102A, the scattering timescales for the FRBs in this sample exceed the expectations from the ISM in our galaxy, implying that the scattering originates far beyond the Milky Way, possibly in the FRB host galaxies. We also do not find any correlations between the scattering timescale and the excess host DM estimates.

In Figure 8, we compare the stellar mass and SFR of the host of FRB 20210117A with those of the FRB host population, and discover that the host has a very low SFR compared to the population. It is evident that: (1) there is little ongoing star formation and there were no bursts of star formation in the past; and (2) the host DM constraints from the Hα measurements rule out excess DM contribution from the host, implying that the majority of the observed excess DM must come from the immediate surroundings of the FRB source. In the same figure, we also compare the stellar masses and SFRs with the hosts of other transients, such as core-collapse supernovae (CCSNe; Schulze et al. 2020), SLSNe (Taggart & Perley 2021), and LGRBs and short GRBs (SGRBs; Taggart & Perley 2021; Nugent et al. 2022). Unlike the dwarf hosts of repeating FRBs, the properties of the FRB 20210117A host do not match those of the SLSNe and LGRB hosts. Furthermore, unlike the hosts of other ASKAP-localized FRBs, the host of FRB 20210117A does not share the same space as the majority of the SGRB hosts. However, it is broadly consistent with the CCSNe hosts.

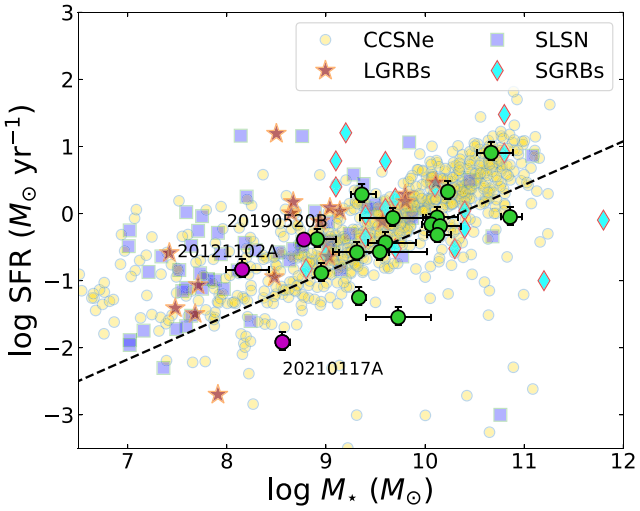

Figure 8. Stellar masses and SFR distributions for FRB hosts compared to the hosts of other transients. The FRB dwarf host galaxies are shown in magenta, while the other FRB hosts are shown in green. The hosts of CCSNe (yellow circles), SLSNe (blue squares), SGRBs (cyan diamonds), and LGRBs (red stars) are overplotted. The dashed line separates star-forming from quiescent galaxies. The data for the transients are taken from Schulze et al. (2020), Taggart & Perley (2021), and Nugent et al. (2022).

5.2. Potential Progenitor Channel

The large DM_{host} of FRB 20210117A strongly hints at the existence of a compact nebula surrounding the FRB engine. Such sources could be powered, for instance, by young pulsars in SN remnants (Connor & Sievers 2016; Piro 2016) or by the interactions of strong winds from a young magnetar with the surrounding medium, forming a pulsar wind nebula (Dai et al. 2017; Margalit & Metzger 2018). A recently proposed scenario, whereby the FRB source is embedded within the powerful baryon-rich outflows from a hyperaccreting black hole ("hyper-nebula"; Sridhar & Metzger 2022; Sridhar et al. 2022), could explain the various properties of FRB 20210117A, including its large DM_{host}. We further investigate this model in the light of our observations.

The derived isotropic equivalent luminosity of the burst seen from FRB 20210117A is $L_{FRB} = 1.36^{+1.06}_{-0.34} \times 10^{43}$ erg s^{-1}. This requires a minimum accretion rate of $\dot{m} = \dot{M}/\dot{M}_{Edd} \gtrsim 10^6$, for the FRB to be accretion jet–powered (Sridhar et al. 2021), where $\dot{M}_{Edd}$ is the Eddington mass transfer rate for an accreting $10M_\odot$ black hole. Such an accretion jet–powered scenario could give rise to repeating—and potentially even periodically active—FRBs, where the periodicity may be associated with the Lense–Thirring precession timescale of the accretion disk/jet passing along the observer's line of sight. In this scenario, the apparent nonrepetition from FRB 20210117A could imply a small

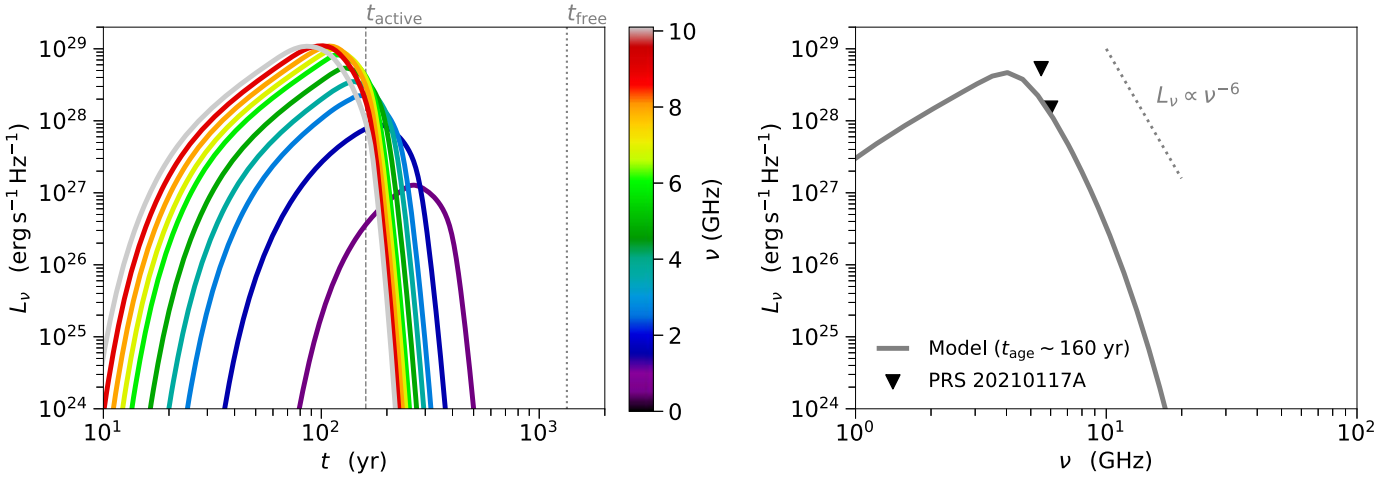

Figure 9. Radio synchrotron emission from an accretion-powered hypernebula surrounding the FRB source. Left: light curves of the expanding hypernebula in different bands (color-coded). The vertical dashed and dotted gray lines denote the active duration of the central accreting engine $t_{\rm active}$ and the free expansion timescale of the hypernebula (Equation (9)), respectively (see Section 5.2 for more details of the system's parameters). Right: spectral energy distribution at the epoch $t_{\rm age} = 160$ yr. The downward-facing black triangles are the upper limits of the PRS associated with FRB 20210117A.

activity duty cycle (Katz 2021; Sridhar et al. 2021):

$$\zeta \approx \left(\frac{4f_{\rm b}}{\pi^2\theta_0^2}\right)^{1/2} \approx \frac{5}{\dot{m}\theta_0} = 5 \times 10^{-5}\left(\frac{\dot{m}}{10^6}\right)^{-1}\left(\frac{\theta_0}{0.1}\right)^{-1}, \quad (8)$$

where $f_{\rm b} = 2\pi(1 - \cos(\Delta\theta))/4\pi \sim 0.01$ is the FRB beaming factor, θ_0 is the angle of the axis of jet precession, and $\Delta\theta$ is the opening angle of the jet.

As they expand, the quasi-spherical disk winds drive a forward shock into the circumstellar medium, with a typical density of, say, $n \approx 10\,{\rm cm}^{-3}$. On the other hand, the faster jet interacts with the slower disk winds via a termination shock. Following Sridhar & Metzger (2022), we calculate the observable properties of the hypernebula due to these interactions for the following physical parameters: the velocity of the slower disk wind $v_{\rm w} = 0.01\,c$; the velocity of the fast wind/jet $v_{\rm j} = 0.1\,c$; the jet magnetization parameter (the ratio of the magnetic energy density to the plasma rest-mass energy density) $\sigma_{\rm j} = 0.1$; the ratio of the wind luminosity to the jet luminosity $\eta = 0.1$; the fraction of the shock power that goes into heating the electrons $\varepsilon_{\rm e} = 0.5$; the mass of the accreting black hole $M_\bullet = 10M_\odot$; and the mass of the companion accretor star $M_\star = 30M_\odot$. The free expansion timescale of the outflowing winds (before they start to decelerate) is

$$t_{\rm free} \approx 1.3 \times 10^3\,{\rm yr}\left(\frac{L_{\rm w,42}}{n_1}\right)^{1/2}\left(\frac{v_{\rm w}}{0.01\,c}\right)^{-2.5}. \quad (9)$$

Above, we adopt the shorthand notation, $Y_x \equiv Y/10^x$, for quantities in cgs units.

During the free expansion phase, the ionized wind shell contributes to a DM through it, as given by Sridhar & Metzger (2022):

$${\rm DM_{sh}} \simeq 470\,{\rm pc\,cm^{-3}}\left(\frac{\dot{m}}{10^6}\right)\left(\frac{v_{\rm w}}{0.01\,c}\right)^{-2}\left(\frac{t_{\rm age}}{160\,{\rm yr}}\right)^{-1}. \quad (10)$$

The model prediction of ${\rm DM_{sh}} \simeq 470\ {\rm pc\,cm^{-3}}$ is consistent with the observed ${\rm DM_{host}} \sim 460\ {\rm pc\,cm^{-3}}$ for our chosen set of parameters. For the same set of parameters, the left panel of Figure 9 shows the model light curves in different bands (0.1–10 GHz). Also indicated there are the active duration of the engine, $t_{\rm active} \approx M_\star/\dot{M} \simeq 150$ yr, and $t_{\rm free}$. The right panel of Figure 9 shows the model spectrum of the radio synchrotron emission from the shock-heated electrons, calculated when the age of the hypernebula is $t_{\rm age} \sim 160$ yr (expansion timescale)—corresponding to the time when the model ${\rm DM_{sh}}$ tentatively matches the observed ${\rm DM_{host}}$. We note here that the model spectrum calculated at this time of expansion is also in agreement with the upper limits on the observed persistent radio emission from FRB 20210117A.

The absolute maximum RM through the nebula at the time $t_{\rm age} \sim 160$ yr is $|{\rm RM}|_{\rm max} \simeq 2 \times 10^7\ {\rm rad\,m^{-2}}$ (Equation (50) of Sridhar & Metzger 2022). The observed RM of $\sim$40 rad m^{-2} is thus consistent within this model, which could mean that the FRB was observed during a phase of RM sign reversal, as has been seen from other FRBs (Anna-Thomas et al. 2022; Dai et al. 2022; Mckinven et al. 2022). Such RM swings could be due to fluctuating orientations of the local magnetic field lines in the turbulent eddies downstream of the termination shock, as would be expected from accreting BH outflows (e.g., Equation (51) of Sridhar & Metzger 2022; see also Yang et al. 2022). Future long-term, short-cadence observations will reveal the trend of $|{\rm RM}|_{\rm max}$ and allow us to better constrain the model parameters, to consistently explain the observed RM(t) as well as the spectra.

6. Summary

We have presented the discovery and subarcsecond localization of the apparently one-off FRB 20210117A, which originates in a dwarf galaxy at $z = 0.214$. The dwarf host galaxy has a little ongoing star formation, as compared to the known dwarf hosts of repeating FRBs. FRB 20210117A is among the sample of FRBs with an excess host DM contribution (${\rm DM_{host}} \sim 460\ {\rm pc\,cm^{-3}}$), where the excess DM is more likely to come from the burst's local environment. The burst is highly (90%) linearly polarized and it has a low RM (43 rad m^{-2}) and a flat polarization PA. A high time resolution analysis of FRB 20210117A and its dynamic spectrum reveals that the burst has three components and a hint of frequency drifting. While none of these characteristics are inconsistent with a nonrepeating origin, flat polarization PAs and frequency

drifting in particular are more commonly found in repeating sources. However, subsequent observations have not detected any repeat bursts. Moreover, we find no radio emission (either a PRS or from star formation) in our follow-up observations. Thus, the local environment of FRB 20210117A is very different to those of the repeating FRBs 20121102A and 20190520B with dwarf host galaxies. Finally, we find that the accretion jet–powered hypernebula model for FRB 20210117A matches with our observations.

We encourage follow-up observations to search for repeating pulses. The discovery of a repeating burst from FRB 20210117A would contradict the observed correlation between FRBs originating in dwarf galaxies and their association with a PRS.

S.B. would like to thank Elizabeth A. K. Adams, Reynier Peletier, Jason Hessels, and the Astroflash group for useful discussions. S.B. is supported by a Dutch Research Council (NWO) Veni Fellowship (VI.Veni.212.058). J.X.P., as a member of the Fast and Fortunate for FRB Follow-up team, acknowledges support from NSF grants AST-1911140, AST-1910471, and AST-2206490. K.W.B., J.P.M, and R.M.S. acknowledge Australian Research Council (ARC) grant DP180100857. R.M.S. acknowledges support through the Australian Research Council Future Fellowship FT190100155 and Discovery Project DP220102305. T.E. is supported by NASA, through the NASA Hubble Fellowship grant HST-HF2-51504.001-A, awarded by the Space Telescope Science Institute, which is operated by the Association of Universities for Research in Astronomy, Inc., for NASA, under contract NAS5-26555. N.S. acknowledges support from NASA (grant No. 80NSSC22K0332), NASA FINESST (grant No. 80NSSC22K1597), and the Columbia University Dean's fellowship. C.W.J. and M.G. acknowledge support from the Australian Government, through the Australian Research Council's Discovery Projects funding scheme (project DP210102103). W.F. and A.C.G. acknowledge support from the National Science Foundation, under CAREER grant No. AST-2047919, and from the David and Lucile Packard Foundation.

Based on observations collected at the European Southern Observatory under ESO program 0105.A-0687. The Australian Square Kilometre Array Pathfinder is part of the Australia Telescope National Facility, which is managed by CSIRO. The operation of ASKAP is funded by the Australian Government, with support from the National Collaborative Research Infrastructure Strategy. ASKAP uses the resources of the Pawsey Supercomputing Centre. The establishment of ASKAP, the Murchison Radio-astronomy Observatory, and the Pawsey Supercomputing Centre are initiatives of the Australian Government, with support from the Government of Western Australia and the Science and Industry Endowment Fund. We acknowledge the Wajarri Yamatji as the traditional owners of the Murchison Radio-astronomy Observatory site. The Australia Telescope Compact Array is part of the Australia Telescope National Facility, which is funded by the Australian Government for operation as a National Facility, managed by CSIRO. We acknowledge the Gomeroi people as the traditional owners of the Observatory site. The National Radio Astronomy Observatory is a facility of the National Science Foundation, operated under cooperative agreement by Associated Universities, Inc. Some of the data presented herein were obtained at the W. M. Keck Observatory, which is operated as a scientific partnership among the California Institute of Technology, the University of California, and the National Aeronautics and Space Administration. The Observatory was made possible by the generous financial support of the W. M. Keck Foundation. Access to the W. M. Keck Observatory was supported by Northwestern University and the Center for Interdisciplinary Exploration and Research in Astrophysics (CIERA). The authors wish to recognize and acknowledge the very significant cultural role and reverence that the summit of Maunakea has always had within the indigenous Hawaiian community. We are most fortunate to have had the opportunity to conduct observations from this mountain.

Facilities: ASKAP, VLA, ATCA, VLT (HAWK-I, FORS2), Keck.

Software: astropy (Astropy Collaboration et al. 2013, 2018), numpy (Harris et al. 2020), matplotlib (Hunter 2007), lmfit (Newville et al. 2016), PyMultiNest (Buchner et al. 2014), bilby (Ashton et al. 2019), fetch (Agarwal et al. 2020), PSRCHIVE (van Straten et al. 2012), miriad (Sault et al. 1995), CASA (McMullin et al. 2007).

ORCID iDs

Shivani Bhandari https://orcid.org/0000-0003-3460-506X
Alexa C. Gordon https://orcid.org/0000-0002-5025-4645
Danica R. Scott https://orcid.org/0000-0002-6895-4156
Lachlan Marnoch https://orcid.org/0000-0003-1483-0147
Navin Sridhar https://orcid.org/0000-0002-5519-9550
Pravir Kumar https://orcid.org/0000-0003-1913-3092
Clancy W. James https://orcid.org/0000-0002-6437-6176
Hao Qiu https://orcid.org/0000-0002-9586-7904
Keith W. Bannister https://orcid.org/0000-0003-2149-0363
Adam T. Deller https://orcid.org/0000-0001-9434-3837
Tarraneh Eftekhari https://orcid.org/0000-0003-0307-9984
Wen-fai Fong https://orcid.org/0000-0002-7374-935X
Marcin Glowacki https://orcid.org/0000-0002-5067-8894
J. Xavier Prochaska https://orcid.org/0000-0002-7738-6875
Stuart D. Ryder https://orcid.org/0000-0003-4501-8100
Ryan M. Shannon https://orcid.org/0000-0002-7285-6348
Sunil Simha https://orcid.org/0000-0003-3801-1496

References

Agarwal, D., Aggarwal, K., Burke-Spolaor, S., Lorimer, D. R., & Garver-Daniels, N. 2020, MNRAS, 497, 1661
Aggarwal, K., Budavári, T., Deller, A. T., et al. 2021, ApJ, 911, 95
Amiri, M., Andersen, B. C., Bandura, K., et al. 2021, ApJS, 257, 59
Anna-Thomas, R., Connor, L., Burke-Spolaor, S., et al. 2022, arXiv:2202.11112
Ashton, G., Hübner, M., Lasky, P. D., et al. 2019, ApJS, 241, 27
Astropy Collaboration, Price-Whelan, A. M., Sipőcz, B. M., et al. 2018, AJ, 156, 123
Astropy Collaboration, Robitaille, T. P., Tollerud, E. J., et al. 2013, A&A, 558, A33
Barsdell, B. R. 2012, PhD thesis, Swinburne Univ. Technology
Berriman, G. B., & Good, J. C. 2017, PASP, 129, 058006
Bhandari, S., Heintz, K. E., Aggarwal, K., et al. 2022, AJ, 163, 69
Bhandari, S., Sadler, E. M., Prochaska, J. X., et al. 2020, ApJL, 895, L37
Buchner, J., Georgakakis, A., Nandra, K., et al. 2014, A&A, 564, A125
Calzetti, D. 2001, PASP, 113, 1449
Chatterjee, S., Law, C. J., Wharton, R. S., et al. 2017, Natur, 541, 58
Chen, G., Ravi, V., & Hallinan, G. W. 2022, arXiv:2201.00999
Cho, H., Macquart, J.-P., Shannon, R. M., et al. 2020, ApJL, 891, L38
Connor, L., Sievers, J., & Pen, U.-L. 2016, MNRAS, 458, L19
Conroy, C. 2013, ARA&A, 51, 393
Conroy, C., & Gunn, J. E. 2010, ApJ, 712, 833

Conroy, C., Gunn, J. E., & White, M. 2009, ApJ, 699, 486
Cordes, J. M., & Lazio, T. J. W. 2002, arXiv:astro-ph/0207156
Cruces, M., Spitler, L. G., Scholz, P., et al. 2021, MNRAS, 500, 448
Dai, S., Feng, Y., Yang, Y. P., et al. 2022, arXiv:2203.08151
Dai, Z. G., Wang, J. S., & Yu, Y. W. 2017, ApJL, 838, L7
Day, C. K., Deller, A. T., James, C. W., et al. 2021, PASA, 38, e050
Day, C. K., Deller, A. T., Shannon, R. M., et al. 2020, MNRAS, 497, 3335
Drlica-Wagner, A., Ferguson, P. S., Adamów, M., et al. 2022, ApJS, 261, 38
Fong, W.-f., Dong, Y., Leja, J., et al. 2021, ApJL, 919, L23
Freudling, W., Romaniello, M., Bramich, D. M., et al. 2013, A&A, 559, 96
Gallazzi, A., Charlot, S., Brinchmann, J., White, S. D. M., & Tremonti, C. A. 2005, MNRAS, 362, 41
Gordon, A. C., Fong, W.-f., Kilpatrick, C. D., et al. 2023, arXiv:2302.05465
Harris, C. R., Millman, K. J., van der Walt, S. J., et al. 2020, Natur, 585, 357
Heintz, K. E., Prochaska, J. X., Simha, S., et al. 2020, ApJ, 903, 152
Hessels, J. W. T., Spitler, L. G., Seymour, A. D., et al. 2019, ApJL, 876, L23
Hilmarsson, G. H., Michilli, D., Spitler, L. G., et al. 2021, ApJL, 908, L10
Hunter, J. D. 2007, CSE, 9, 90
James, C. W., Ghosh, E. M., Prochaska, J. X., et al. 2022a, MNRAS, 516, 4862
James, C. W., Prochaska, J. X., Macquart, J. P., et al. 2022b, MNRAS, 509, 4775
James, P. A., Shane, N. S., Beckman, J. E., et al. 2004, A&A, 414, 23
Johnson, B. D., Leja, J., Conroy, C., & Speagle, J. S. 2021, ApJS, 254, 22
Kaisin, S. S., Karachentsev, I. D., & Ravindranath, S. 2012, MNRAS, 425, 2083
Katz, J. I. 2021, MNRAS, 502, 4664
Kirsten, F., Marcote, B., Nimmo, K., et al. 2022, Natur, 602, 585
Kriek, M., & Conroy, C. 2013, ApJL, 775, L16
Kroupa, P. 2001, MNRAS, 322, 231
Kumar, P., Shannon, R. M., Flynn, C., et al. 2021, MNRAS, 500, 2525
Lang, D., Hogg, D. W., Mierle, K., Blanton, M., & Roweis, S. 2010, ApJ, 139, 1782
Lee, K.-G., Ata, M., Khrykin, I. S., et al. 2022, ApJ, 928, 9
Leja, J., Carnall, A. C., Johnson, B. D., Conroy, C., & Speagle, J. S. 2019, ApJ, 876, 3
Li, D., Wang, P., Zhu, W. W., et al. 2021, Natur, 598, 267
Lindegren, L., Hernández, J., Bombrun, A., et al. 2018, A&A, 616, A2
Macquart, J. P., Prochaska, J. X., McQuinn, M., et al. 2020, Natur, 581, 391
Macquart, J.-P., Shannon, R. M., Bannister, K. W., et al. 2019, ApJL, 872, L19
Marcote, B., Nimmo, K., Hessels, J. W. T., et al. 2020, Natur, 577, 190
Marcote, B., Paragi, Z., Hessels, J. W. T., et al. 2017, ApJL, 834, L8
Margalit, B., Berger, E., & Metzger, B. D. 2019, ApJ, 886, 110
Margalit, B., & Metzger, B. D. 2018, ApJL, 868, L4
Marnoch, L., Ryder, S. D., Bannister, K. W., et al. 2020, A&A, 639, A119
McConnell, D., Hale, C. L., Lenc, E., et al. 2020, PASA, 37, e048
Mckinven, R., Gaensler, B. M., Michilli, D., et al. 2022, arXiv:2205.09221
McMullin, J. P., Waters, B., Schiebel, D., Young, W., & Golap, K. 2007, in ASP Conf. Ser. 376, Astronomical Data Analysis Software and Systems XVI, ed. R. A. Shaw, F. Hill, & D. J. Bell (San Francisco, CA: ASP), 127
Michilli, D., Seymour, A., Hessels, J. W. T., et al. 2018, Natur, 553, 182
Newville, M., Stensitzki, T., Allen, D. B., et al. 2016, Lmfit: Non-Linear Least-Square Minimization and Curve-Fitting for Python, Astrophysics Source Code Library, ascl:1606.014
Niu, C. H., Aggarwal, K., Li, D., et al. 2022, Natur, 606, 873
Nugent, A. E., Fong, W.-f., Dong, Y., et al. 2022, ApJ, 940, 57
Petroff, E., Barr, E. D., Jameson, A., et al. 2016, PASA, 33, e045
Piro, A. L. 2016, ApJL, 824, L32
Pleunis, Z., Good, D. C., Kaspi, V. M., et al. 2021, ApJ, 923, 1
Prochaska, J., Hennawi, J., Westfall, K., et al. 2020, JOSS, 5, 2308
Prochaska, J. X., & Zheng, Y. 2019, MNRAS, 485, 648
Qiu, H., Shannon, R. M., Farah, W., et al. 2020, MNRAS, 497, 1382
Ravi, V., Catha, M., Addario, L. D., et al. 2019, Natur, 572, 352
Ravi, V., Catha, M., Chen, G., et al. 2022, arXiv:2211.09049
Ryder, S. D., Bannister, K. W., Bhandari, S., et al. 2022, arXiv:2210.04680
Salpeter, E. E. 1966, AJ, 71, 869
Sault, R. J., Teuben, P. J., & Wright, M. C. H. 1995, in ASP Conf. Ser. 77, Astronomical Data Analysis Software and Systems IV, ed. R. A. Shaw, H. E. Payne, & J. J. E. Hayes (San Francisco, CA: ASP), 433
Schulze, S., Yaron, O., Sollerman, J., et al. 2020, ApJS, 255, 29
Shannon, R. M., Macquart, J.-P., Bannister, K. W., et al. 2018, Natur, 562, 386
Simha, S., Lee, K.-G., & Prochaska, J. X. 2023, arXiv:2303.07387
Skrutskie, M. F., Cutri, R. M., Stiening, R., et al. 2006, AJ, 131, 1163
Speagle, J. S. 2020, MNRAS, 493, 3132
Spitler, L. G., Scholz, P., Hessels, J. W. T., et al. 2016, Natur, 531, 202
Sridhar, N., & Metzger, B. D. 2022, ApJ, 937, 5
Sridhar, N., Metzger, B. D., Beniamini, P., et al. 2021, ApJ, 917, 13
Sridhar, N., Metzger, B. D., & Fang, K. 2022, arXiv:2212.11236
Sutinjo, A. T., Scott, D. R., James, C. W., et al. 2023, arXiv:2302.06220
Taggart, K., & Perley, D. A. 2021, MNRAS, 503, 3931
Tendulkar, S. P., Bassa, C. G., Cordes, J. M., et al. 2017, ApJL, 834, L7
van Straten, W., Demorest, P., & Oslowski, S. 2012, AR&T, 9, 237
Xu, H., Niu, J. R., Chen, P., et al. 2022, Natur, 609, 685
Xu, J., & Han, J. L. 2015, RAA, 15, 1629
Yang, Y.-P., Xu, S., & Zhang, B. 2023, MNRAS, 520, 2039–2054
Yao, J. M., Manchester, R. N., & Wang, N. 2017, ApJ, 835, 29